Brain Perfusion Analysis Method using Computed Tomography Images

Ekaterina Khudiakova[1], Andrey Gavrilov[2], Andrey Krylov[1]

[1] Laboratory of Mathematical Methods of Image Processing, Faculty of Computational Mathematics and Cybernetics, Lomonosov Moscow State University – Moscow, Russia – hudyakovakate@gmail.com , kryl@cs.msu.su
[2] Research Department, Gammamed-Soft, Ltd. – Moscow, Russia – agavrilov49@gmail.com

Keywords: Perfusion, Computed Tomography, Self-Supervised, Denoising, AIF, Noise2Noise.

Abstract

In this paper, a multi-stage perfusion calculation pipeline is suggested. It contains preprocessing algorithms for brain tissue segmentation, input artery and output vein detection, a self-supervised neural network for CT image denoising, and regularization deconvolution methods. SVD and TTV-based regularization methods were used at the last stage. The results of the comparison of these methods to classical SVD and TTV ones show that the self-supervised method outperforms others both for simulation and real data. For simulation, RMSE and SSIM metrics were used for comparison, and as for the real data, CNR metrics were compared for lesion and normal white matter areas, and for the latter ones bias and standard deviation were calculated.

1. Introduction

Perfusion computed tomography or CT perfusion is a technique for the dynamic study of blood flow parameters. When performing computed tomography, a contrast agent is injected, and then scanning is performed. The data obtained are then processed to obtain perfusion maps with various parameters such as CBV (Cerebral Blood Volume), CBF (Cerebral Blood Flow), MTT (Mean Transit Time), and TTP (Time To Peak). This type of research is used to diagnose acute ischemic cerebral circulation disorders, which are one of the leading causes of morbidity, mortality, and disability worldwide. Since the calculation of perfusion map values is based on the problem of deconvolution, which is ill-posed, it is necessary to use various regularization methods.

While classical methods of noise filtration (See Section 5) may be used for that, one could also use neural network approaches. One way is to train a simple neural network using simulation data. However, there is a limited number of high-quality simulations for brain perfusion, and the resulting neural network may not work stable for unusual situations.

As perfusion data are essentially a 3D time-series data, with contrast gradually passing in time, it is possible to use this fact to train a neural network, if it is considered that most adjacent images differ by small value of contrast concentration. Further details of neural network proposed may be found in Section 6.

The described network is compared with well-studied classical deconvolution methods of SVD and TTV.

2. Perfusion Model

Perfusion model and calculation details are described in (König, 2003), (Konstas et al., 2009a), (Konstas et al., 2009b). The notations of the main model functions are shown in Table 1.

The difference between the intensities of the CT scan of a brain with contrast agent and without it is considered to be proportional to the concentration of the contrast agent. Several image voxels are marked as arterial ones. The concentration corresponding to their mean value is denoted as $c_{art}(t)$. For each voxel (volume of interest) the residual function $k(t)$ is introduced so that it is related to the concentration of the contrast agent in the volume of interest in the following way:

Description	Variable	Unit
Contrast concentration in artery	c_{art}	g/ml
Contrast concentration in volume of interest	c_{voi}	g/ml
Average density in volume of interest	ρ_{voi}	g/ml
Intermediate variable	$k(t)$	1/s
Cerebral Blood Flow	CBF	ml/100g/s
Cerebral Blood Volume	CBV	ml/100g
Mean Transit Time	MTT	s

Table 1. Table of symbols.

$$c_{voi}(t) = (c_{art} * k)(t). \tag{1}$$

Then, the values for perfusion maps are calculated as follows:

$$CBF = \frac{1}{\rho_{voi}} max(k(t)), \tag{2}$$

$$CBV = \frac{1}{\rho_{voi}} \int_0^\infty k(\tau) d\tau, \tag{3}$$

$$MTT = \frac{1}{max(k(t))} \int_0^\infty k(\tau) d\tau = \frac{CBV}{CBF}. \tag{4}$$

Hence, the problem is reduced to calculating the function $k(t)$. To use this model for real data, the values are considered on a discrete grid, and the final problem can be written as follows:

$$Ak = c, \tag{5}$$

where $$A = \Delta t \cdot \begin{pmatrix} c_{art}(t_1) & 0 & \dots & 0 \\ c_{art}(t_2) & c_{art}(t_1) & \dots & 0 \\ \vdots & \vdots & \ddots & \vdots \\ c_{art}(t_N) & c_{art}(t_{N-1}) & \dots & c_{art}(t_1) \end{pmatrix},$$

This contribution has been peer-reviewed. The double-blind peer-review was conducted on the basis of the full paper.
https://doi.org/10.5194/isprs-annals-X-2-W1-2024-9-2024 | © Author(s) 2024. CC BY 4.0 License.

$$k = (k(t_1), k(t_2), ..., k(t_N))^T,$$
$$c = (c_{voi}(t_1), c_{voi}(t_2), ..., c_{voi}(t_N)))^T.$$

A number of studies ((Wittsack et al., 2008), (Sasaki et al., 2009)) show that in order to reduce the effect of bolus delay and make the solution independent of time shifts on the time concentration curve in the tissue, a block-circulant matrix can be used, with supplementing the vector $c_{art}(t)$ by zeros to the desired size. The block-circulant matrix is as follows:

$$\tilde{A} = \begin{pmatrix} A & B \\ B & A \end{pmatrix} \tag{6}$$

where $$B = \Delta t \cdot \begin{pmatrix} 0 & c_{art}(t_N) & ... & c_{art}(t_2) \\ 0 & 0 & ... & c_{art}(t_3) \\ \vdots & \vdots & \ddots & \vdots \\ 0 & 0 & ... & 0 \end{pmatrix}.$$

The new equation:

$$\tilde{A}\tilde{k} = \tilde{c}. \tag{7}$$

The notation (A, k, c) will be used further, since the following is true for both cases.

3. Data

To test the algorithm, the phantom data (Aichert et al., 2013), the ISLES2018 dataset ((Kistler et al., 2013), (Maier et al., 2017)), and 18 CT brain images obtained from MultiVox company were used. Examples of slices are shown in Fig. 1.

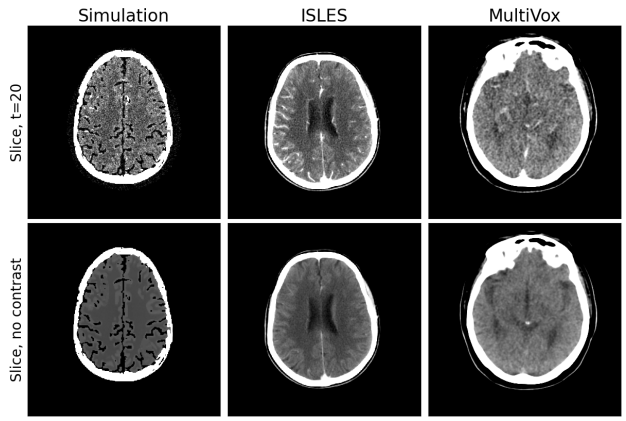

Figure 1. Slices for different datasets before and after contrast agent injection.

3.1 Phantom

Phantom is a simulation of brain CT perfusion, one series of 4D data $256 \times 256 \times 256 \times 50$ (in three spatial coordinates and in time). For each slice areas of reduced perfusion can be marked manually using MATLAB software.

50 slices (101-150) were used for training, 15 (156-170) for validation. 5 slices between training and validation data were not used to reduce the correlation between them.

Poisson and Gaussian noise were added to initial images to test the work of algorithms. Noise was added to the x image using the following formula:

$$Image\ (\sigma, \gamma) = \frac{Poisson(\gamma * (x + Gaussian(\mu, \sigma)))}{\gamma} \tag{8}$$

For this work, the values $\mu = 0$, $\sigma = 10$, $\gamma = 0.1$ were used.

In addition to the generated perfusion data, reference perfusion maps (CBF, CBV, MTT) are also available.

3.2 ISLES2018

The ISLES2018 dataset contains 94 CT series, for each of the patients CT scan of brain with dynamic contrast is available (4D images $n \times 256 \times 256 \times 49$). 17 series were selected for network training, and 5 for validation. Perfusion maps calculated for each series are also available. However, unlike Phantom data, these maps were not used as reference ones, since noise was not generated on these data, and the maps are not absolutely true, but represent data calculated using one of the described methods (see 5.1).

3.3 MultiVox

18 CT scans are presented as examples of data that will need to be processed by the Multivox software, using the implemented code. Each scan is a set of images with the format of $n \times 512 \times 512 \times t$.

4. Data Preprocessing

4.1 Segmentation of Brain Tissues

Segmentation of brain tissues is performed using the information about the characteristic values of density for various tissues (Table 2).

Substance	HU (Hounsfield Units)
Air	-1000
Cerebrospinal fluid	15
Gray matter	from 30 to 45
White matter	20 to 30
Blood	from 30 to 70
Bone	from 300 to 1000
Contrast agent (arterial phase)	from 100 to 300
Contrast agent (venous phase)	from 70 to 150

Table 2. Values for different substances.

Thresholds and classical mathematical morphological operations were used for segmentation maps calculation.

4.2 Arterial Input Function

The Venous Output Function (VOF) is calculated using the method proposed in (Kao et al., 2014). The Arterial Input Function (AIF) is found by the method proposed in (Mouridsen et al., 2006). They mainly involve analyzing area under curve, first and second moment for curves of contrast agent concentration for each voxel. As for AIF, this process is followed by several iterations of clusterization, and the cluster with the minimal first momentum is chosen each time. As a result, several voxels are selected as arterial ones.

Fig. 2 shows the obtained function values and marked voxels for two slices from the datasets.

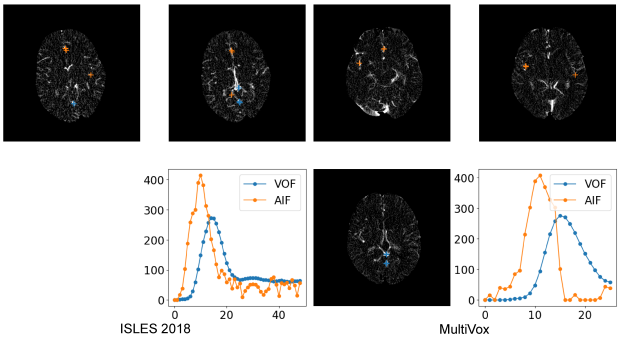

Figure 2. Arterial Input Function.

5. Classical Methods

5.1 tSVD

Using the singular value decomposition of the matrix A (Equation 5), we obtain

$$A = U\Sigma V^T = \sum_{i=1}^{r} u_i \sigma_i v_i^T, \tag{9}$$

$$k_{ls} = \sum_{i=1}^{r} \frac{u_i c}{\sigma_i} v_i, \tag{10}$$

$$k_{ls} = argmin(\| Ak - c \|_2^2), k \in R^N. \tag{11}$$

However, in case of an ill-conditioned matrix A, such a solution will be unstable to small changes in the vector c. To obtain a numerically stable result, various regularization methods can be used.

In order for the solution to be stable, the method of truncated decomposition of singular values, tSVD (Fieselmann et al., 2011) can be used. In this approach, small singular values are discarded:

$$k_\lambda = \sum_{i=1}^{r} (f_{\lambda,i} \frac{u_i c}{\sigma_i}) v_i, \tag{12}$$

where $$f_{\lambda,i} = \begin{cases} 0, \sigma_i < \lambda, \lambda = \lambda_{rel} * \sigma_1, \\ 1, \sigma_i > \lambda \end{cases}.$$

To reduce the effect of noise, images are also pre-blurred with a Gaussian filter.

5.2 Tensor Total Variation

Since CT scans of brain are usually quite noisy, the above mentioned method may not give sufficient effect. One of the common ways of regularization is also the use of Tensor Total Variation, or TTV (Fang et al., 2015). In this method, strong changes in the neighboring values of the desired function are penalized, and thus its smoothness is achieved:

$$K = \underset{K}{argmin}(\frac{1}{2} \| AK - C \|_2^2 + \| K \|_{TV}), \tag{13}$$

where $$\| K \|_{TV} = \sum_{t,i,j,k} (\gamma_1 |K_{t+1,i,j,k} - K_{t,i,j,k}| + \gamma_2 (|K_{t,i+1,j,k} - K_{t,i,j,k}| + |K_{t,i,j+1,k} - K_{t,i,j,k}| + |K_{t,i,j,k+1} - K_{t,i,j,k}|)),$$
$K \in \mathbb{R}^{T \times I \times J \times K}$.

In case of perfusion, one of the spatial coordinates is rather sparse, so no regularization is performed on it:

$$\| K \|_{TV} = \sum_{t,i,j,k} (\gamma_1 |K_{t+1,i,j,k} - K_{t,i,j,k}| + \gamma_2 (|K_{t,i+1,j,k} - K_{t,i,j,k}| + |K_{t,i,j+1,k} - K_{t,i,j,k}|)) \tag{14}$$

In this method, it is necessary to vary the parameters of γ_i, which in practice presents considerable complexity and strongly affects the result of calculations, especially given the lack of reference maps for real data. In case of using images from different devices with different noise levels, it becomes necessary to select these values manually.

Algorithm 1 Gradient descent algorithm using TTV.

Entrance: regularization parameters λ, γ.
Exit: function $K \in \mathbb{R}^{T \times N_1 \times N_2}$.
$K^0 = 0, t^1 = r^1 = K^0$
for $n = 1, 2, ..., N$ **do:**
  Gradient descent:
    $Q_1 = A^T \cdot (A \cdot r^n - c), Q_2 = \lambda \times r^n,$
    $s = \frac{\sum (Q_1 + Q_2)^2}{\sum (AQ_1^2 + \lambda Q_2^2)},$
    $K_p = r^n - s \cdot (Q1 + Q2).$
  Regularization:
    $K^n = prox_\gamma (2 \| K \|_{TV})(K_g),$
    $prox_\rho(g)(x) = \underset{u}{argmin}\{g(u) + \frac{1}{2\rho} \| u - x \|\}.$
  Update t, r**:**
    $t^{n+1} = \frac{1 + \sqrt{1 + 4(t^n)^2}}{2},$
    $r^{n+1} = K^n + \frac{t^n - 1}{t^{n+1}} (K^n - K^{n-1}).$

Stochastic gradient descent (Algorithm 1) is used to find the matrices. The $prox$ function is calculated using the proxtv library ((Barbero and Sra, 2011), (Barbero and Sra, 2018)).

5.3 Other Classical Methods

In addition to Gaussian filters, there are other filtering methods that allow to remove noise from the image to some extent (Gabor filtering, median filtering, etc.). An overview of such methods is given in (El-Shafai et al., 2023).

In addition to TTV, other additional regularization parameters for gradient descent can be used to calculate perfusion maps using variation methods.

For example, in (Lyukov et al., 2019), in addition to the first derivative, the second one is also involved (Total Generalized Variation, TGV).

In (Zeng et al., 2016), (Wu et al., 2020), a Structure Total Variation (STV, (Lefkimmiatis et al., 2015)) is used. This method uses information about the voxel environment obtained from the eigenvalues of the structure tensor.

6. Noise2Noise

The use of a Gaussian filter before applying tSVD significantly reduces the local accuracy in calculating perfusion maps, and cannot always effectively suppress noise. One of the alternatives to solve the problems that arise is the use of neural network methods to obtain less noisy images. In this paper, we consider the Noise2Noise ((Lehtinen et al., 2018)) neural network based on the classical UNet architecture (Fig. 3, Fig. 4). In addition to the standard architecture, padding (image addition to preserve dimension after applying convolution) and a Batch Normalization layer were added.

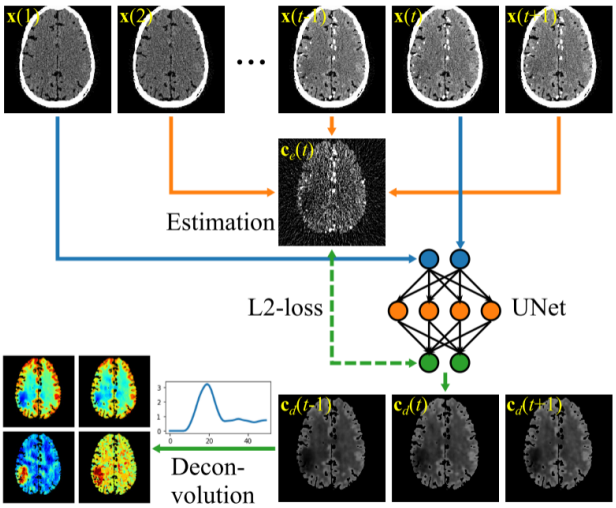

Figure 3. Noise2Noise pipeline.

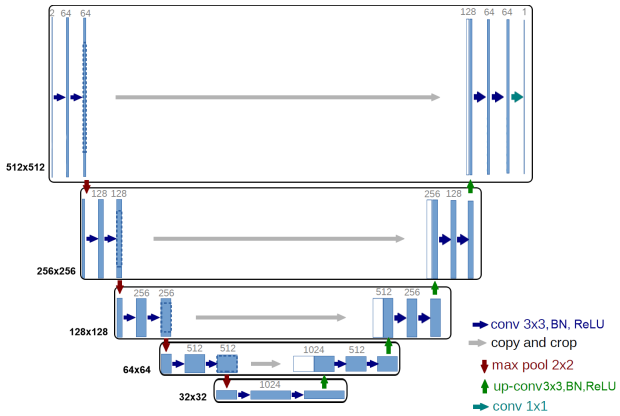

Figure 4. UNet architecture.

The method is proposed in (Wu et al., 2021). To use Noise2Noise, noisy images $x + n_1$, $x + n_2$ (n_i is noise) are fed to both input and output, such that n_1, n_2 have zero mean and do not depend on each other.

Contrast agent concentration is considered to be proportional to $c(t)$, where $c(t)$ is as follows:

$$c(t) = x(t) - \sum_{t_0=1}^{T} x(t_0), \tag{15}$$

where $x(t)$ = slice at time t.

In this research $T = 2$ is taken. Since $c(t)$ represents the propagation of contrast agent over time with fixed time intervals, then

$$c(t) \approx \frac{c(t+1) + c(t-1)}{2}. \tag{16}$$

To apply a neural network, it is necessary that the noise in the original image be independent of the noise of the approximate image, but if the noise for neighboring slices $x(t-1)$, $x(t)$, $x(t+1)$ can be considered independent, then the presence of the same value $\sum_{t_0=1}^{T} x(t_0)$ for each of $c(t)$ gives noise with non-zero correlation. Therefore, instead of the average value, slices at different points in time t_0 are used to obtain images:

$$x(t) - x(1) \approx \frac{x(t-1) + x(t+1)}{2} - x(2). \tag{17}$$

However, it is also necessary that the average noise value be zero, so the following estimation is used:

$$x_e(t) = k(t)\frac{x(t-1) + x(t+1)}{2}, \tag{18}$$

where $k(t) = \underset{k}{argmin}||k\frac{x(t-1)+x(t+1)}{2} - x(t)||_2^2$.

Thus, the following main loss function is used:

$$L_{n2n}(\Theta) = \frac{1}{2N}\sum_{i=1}^{N}\frac{1}{T_i - 2}\sum_{t=2}^{T_i-1}\sum_{t_0=1}^{2}||f(x_i(t), x_i(t_0); \Theta) - \\ - (x_{ie}(t) - x_i(3 - t_0))||_2^2. \tag{19}$$

But using $x_e(t)$ shifts the noise distribution, so additional regularization needs to be used. Since noise is usually high-frequency information, the following loss function is used to save low-frequency information (after applying strong Gaussian filtering, the image submitted to the input and one obtained using a neural network are compared):

$$L_{bias}(\Theta) = \frac{1}{2N}\sum_{i=1}^{N}\frac{1}{T_i - 2}\sum_{t=2}^{T_i-1}\sum_{t_0=1}^{2}||G * f(x_i(t), x_i(t_0); \Theta) - \\ - G * (x_i(t) - x_i(t_0)||_2^2. \tag{20}$$

The final loss function is calculated as

$$\Theta^* = \underset{\Theta}{argmin}(L_{n2n}(\Theta) + \beta L_{bias}(\Theta)). \tag{21}$$

The use of $x_e(t)$ has the greatest impact at time points close to the peak concentration of the contrast agent, since the approximation by neighboring slices at this time is the least accurate.

At the same time, these points carry out important information for the final calculation of perfusion parameters, but their percentage in the training data is not so large. Therefore, it is also proposed to choose the time interval unevenly, and use more slices near the peak concentration during the training process. The peak concentration time is calculated using the formula

$$t_{peak} = \underset{t}{argmax}(x(t)). \tag{22}$$

After obtaining the concentration of the contrast agent, it is also necessary to solve the problem of deconvolution. In this paper, we consider the combination of Noise2Noise with the above described methods of tSVD and TTV.

7. Results

The results of calculations using various deconvolution methods for Phantom data are shown in Fig. 5. Without filtering, the resulting maps turn out to be completely uninformative. The usage of TTV method results in a large number of block artifacts, as borders of zones with different values tend to be straight lines. Maps obtained using Gaussian filtering lack accuracy in comparison with Noise2Noise. A visual comparison of the residual function $k(t)$ in one of the voxels confirms that the neural network method allows one to get the desired function in the closest way to the original one.

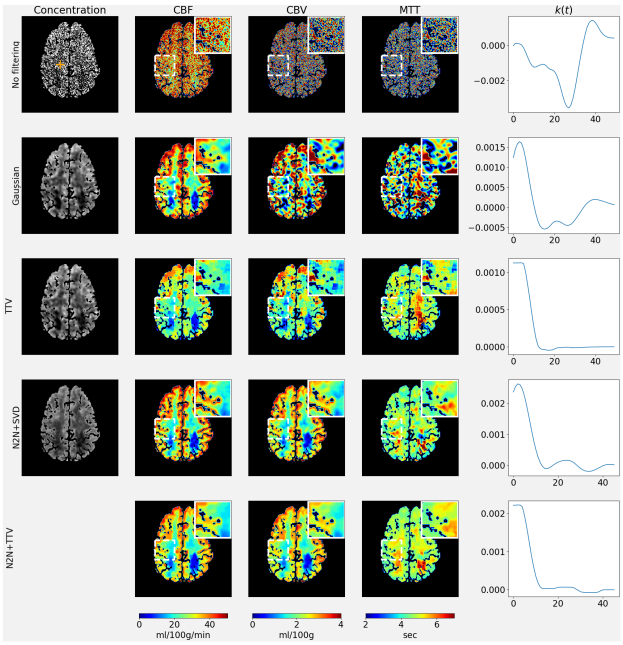

Figure 5. Results, Phantom.

The same is shown when comparing the obtained maps with the reference ones (Fig. 6) according to the RMSE and SSIM metrics. For all perfusion maps, the RMSE metric decreased significantly compared to other methods, and the SSIM increased when using Noise2Noise with tSVD. At the same time, for the neural network method with TTV, the metrics for CBF show a slightly worse result, and for MTT significantly better. According to the residual functions, the use of the first derivative in this case may have led to excessive smoothing. This may be due to the fact that for Phantom data, neural network training took place on homogeneous noise and similar data, as a result

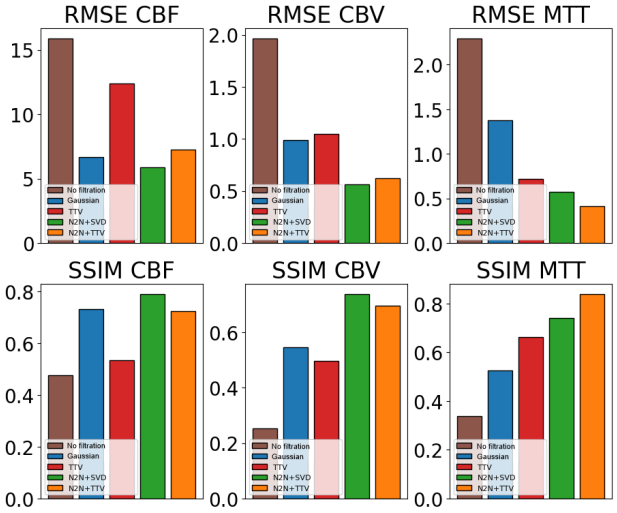

Figure 6. Metrics, Phantom.

of which Noise2Noise itself coped well with the task, and the use of additional regularization was not needed.

In Fig. 7, 9 the results of map calculations for ISLES2018 and MultiVox data, respectively, are presented. The results are mostly the same as for Phantom data - maps are unreadable without filtering, using TTV leads to block artifacts, which is most noticeable for MultiVox data. Noise2Noise copes best with calculating maps and greatly increases resolution. However, after applying regularization by the method of tSVD, the residual function is still subject to noise, which is especially noticeable on MultiVox data. Using the TTV allows one to further denoise the residual function.

For ISLES dataset, CNR metric (23) was calculated for lesion area compared to normal white matter for MTT maps (See 3). It shows that neural network methods cope significantly better with the task of distinguishing the areas, and confirm the conclusion that using TTV after denoising may lead to unnecessary smoothing.

$$CNR = \frac{S_{lesion} - S_{normal}}{\sigma_{normal}}, \tag{23}$$

where S_{lesion} = mean value of voxel intensities for MTT map in lesion area,
S_{normal} = mean value of voxel intensities for MTT map in normal white matter area,
σ_{normal} = standard deviation of voxel intensities for MTT map in normal white matter area.

Method	Contrast	Noise	CNR
No filtration	0.218	8.448	0.026
Gaussian	1.317	1.436	0.917
TTV	3.077	24.137	0.127
N2N+SVD	1.779	1.106	1.609
N2N+TTV	3.038	2.448	1.241

Table 3. Values for different substances.

Bias and standard deviation for normal white matter were also calculated for both ISLES2018 and MultiVox. Bias was calculated by averaging values of obtained concentration maps at each time point and subtracting same value for initial noisy concentration maps. The use of neural network significantly reduces bias, and standard deviation mainly stays on the same

level. It should be noted that these values cannot be calculated for TTV-based methods, as TTV does not provide denoised concentration maps.

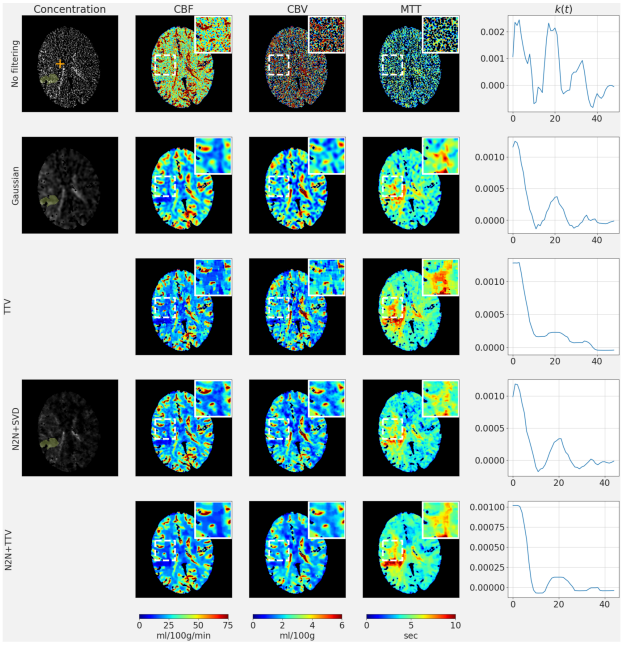

Figure 7. Results, ISLES2018.

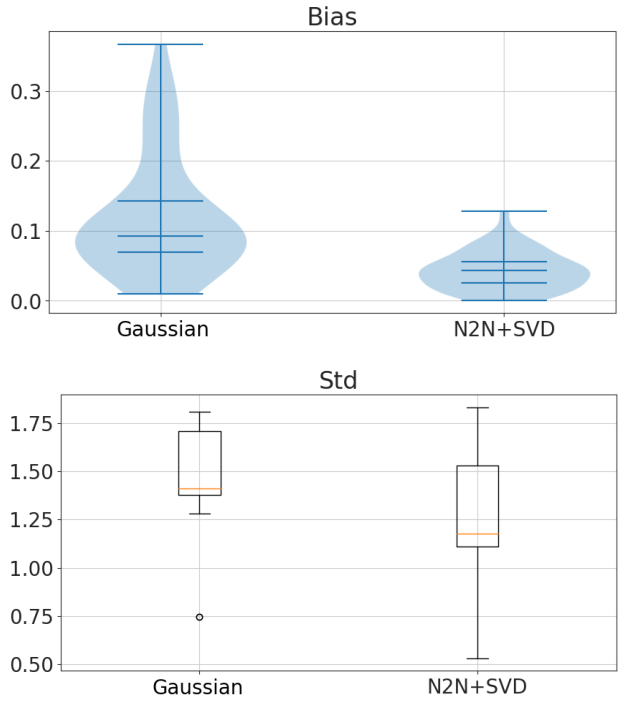

Figure 8. Bias and standard deviation for normal white matter areas, ISLES2018.

8. Conclusions

Algorithms have been developed for pre-processing CT series: finding the mask of brain tissues using mathematical morphology, and finding the arterial input function using cluster curve analysis. Two deconvolution algorithms were also implemented to obtain perfusion maps using tSVD and TTV.

Using the Noise2Noise architecture, a neural network was trained to reduce noise in images before applying deconvolution, and its operation on various datasets using both of the above mentioned algorithms was investigated.

The resulting algorithm has significantly improved the resolution of perfusion maps and the quality of their calculation. It has shown best results for simulation data when compared by MSE and SSIM metrics, and for ISLES2018 data, with significantly better CNR metric.

References

Aichert, A., Manhart, M., Navalpakkam, B., Grimm, R., Hutter, J., Maier, A., Hornegger, J., Doerfler, A., 2013. A realistic digital phantom for perfusion C-arm CT based on MRI data. *IEEE Nuclear Science Symposium Conference Record*, 1-2.

Barbero, A., Sra, S., 2011. Fast newton-type methods for total variation regularization. *International Conference on Machine Learning*, 313–320.

Barbero, A., Sra, S., 2018. Modular Proximal Optimization for Multidimensional Total-Variation Regularization. *Journal of Machine Learning Research*, 19(56), 1-82.

El-Shafai, W., El-Nabi, S. A., Ali, A. M., El-Rabaie, E. S. M., El-Samie, F. E. A., 2023. Traditional and deep-learning-based denoising methods for medical images. *Multimedia Tools and Applications*, 83, 1-28.

Fang, R., Zhang, S., Chen, T., Sanelli, P. C., 2015. Robust Low-Dose CT Perfusion Deconvolution via Tensor Total-Variation Regularization. *IEEE Transactions on Medical Imaging*, 34, 1533-1548.

Fieselmann, A., Kowarschik, M., Ganguly, A., Hornegger, J., Fahrig, R., 2011. Deconvolution-based CT and MR brain perfusion measurement: theoretical model revisited and practical implementation details. *Journal of Biomedical Imaging*, 2011, 1–20.

Kao, Y. H., Teng, M. M. H., Kao, Y. T., Chen, Y. J., Wu, C. H., Chen, W. C., Chiu, F. Y., Chang, F. C., 2014. Automatic measurements of arterial input and venous output functions on cerebral computed tomography perfusion images: A preliminary study. *Computers in Biology and Medicine*, 51, 51-60.

Kistler, M., Bonaretti, S., Pfahrer, M., Niklaus, R., Büchler, P., 2013. The virtual skeleton database: An open access repository for biomedical research and collaboration. *Journal of Medical Internet Research*, 15, e245.

Konstas, A. A., Goldmakher, G. V., Lee, T. Y., Lev, M. H., 2009a. Theoretic basis and technical implementations of CT perfusion in acute ischemic stroke, part 1: Theoretic basis. *American Journal of Neuroradiology*, 30, 662–668.

Konstas, A. A., Goldmakher, G. V., Lee, T. Y., Lev, M. H., 2009b. Theoretic basis and technical implementations of CT perfusion in acute ischemic stroke, Part 2: Technical implementations. *American Journal of Neuroradiology*, 30, 885-892.

König, M., 2003. Brain perfusion CT in acute stroke: Current status. *European Journal of Radiology*, 45, S11-S22.

Lefkimmiatis, S., Roussos, A., Maragos, P., Unser, M., 2015. Structure Tensor Total Variation. *SIAM Journal on Imaging Sciences*, 8, 1090-1122.

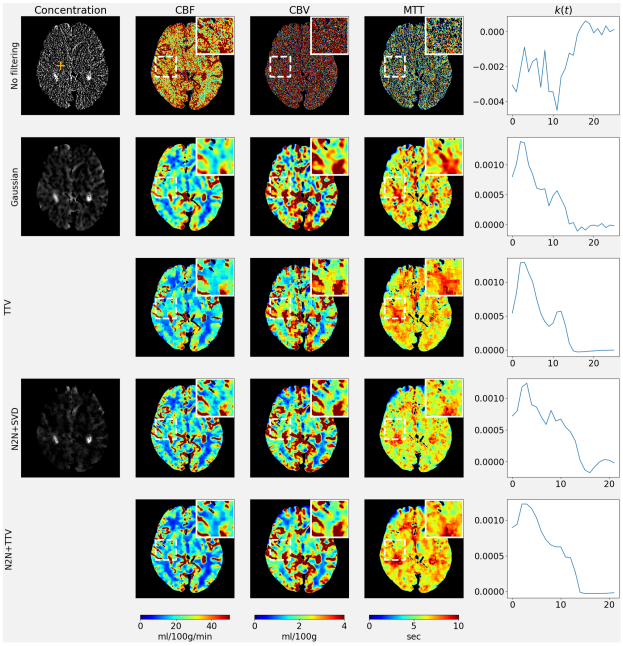

Figure 9. Results, MultiVox.

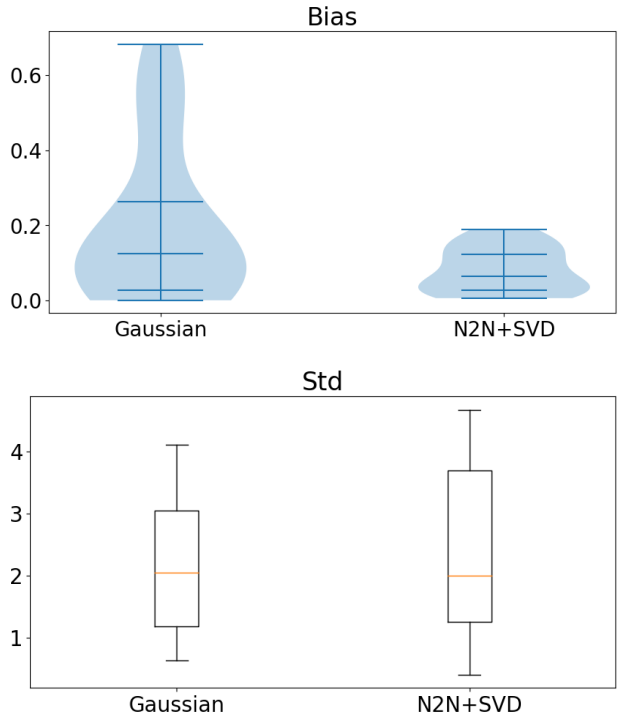

Figure 10. Bias and standard deviation for normal white matter areas, MultiVox.

Lehtinen, J., Munkberg, J., Hasselgren, J., Laine, S., Karras, T., Aittala, M., Aila, T., 2018. Noise2Noise: Learning image restoration without clean data. *35th International Conference on Machine Learning, ICML 2018*, 7.

Lyukov, D. A., Krylov, A. S., Lukshin, V. A., 2019. Total generalized variation method for deconvolution-based CT brain perfusion. *CEUR Workshop Proceedings*, 2485, 136-139.

Maier, O., Menze, B. H., von der Gablentz, J., Häni, L., Heinrich, M. P., Liebrand, M., Winzeck, S., Basit, A., Bentley, P., Chen, L., Christiaens, D., Dutil, F., Egger, K., Feng, C., Glocker, B., Götz, M., Haeck, T., Halme, H. L., Havaei, M., Iftekharuddin, K. M., Jodoin, P. M., Kamnitsas, K., Kellner, E., Korvenoja, A., Larochelle, H., Ledig, C., Lee, J. H., Maes, F., Mahmood, Q., Maier-Hein, K. H., McKinley, R., Muschelli, J., Pal, C., Pei, L., Rangarajan, J. R., Reza, S. M., Robben, D., Rueckert, D., Salli, E., Suetens, P., Wang, C. W., Wilms, M., Kirschke, J. S., Krämer, U. M., Münte, T. F., Schramm, P., Wiest, R., Handels, H., Reyes, M., 2017. ISLES 2015 - A public evaluation benchmark for ischemic stroke lesion segmentation from multispectral MRI. *Medical Image Analysis*, 35, 250-269.

Mouridsen, K., Christensen, S., Gyldensted, L., Østergaard, L., 2006. Automatic selection of arterial input function using cluster analysis. *Magnetic Resonance in Medicine*, 55, 524-531.

Sasaki, M., Kudo, K., Ogasawara, K., Fujiwara, S., 2009. Tracer Delay–Insensitive Algorithm Can Improve Reliability of CT Perfusion Imaging for Cerebrovascular Steno-Occlusive Disease: Comparison with Quantitative Single-Photon Emission CT. *American Journal of Neuroradiology*, 30(1), 188–193.

Wittsack, H. J., Wohlschläger, A. M., Ritzl, E. K., Kleiser, R., Cohnen, M., Seitz, R. J., Mödder, U., 2008. CT-perfusion imaging of the human brain: Advanced deconvolution analysis using circulant singular value decomposition. *Computerized Medical Imaging and Graphics*, 32, 67-77.

Wu, D., Ren, H., Li, Q., 2021. Self-Supervised Dynamic CT Perfusion Image Denoising with Deep Neural Networks. *IEEE Transactions on Radiation and Plasma Medical Sciences*, 5, 350-361.

Wu, J., Wang, X., Mou, X., Chen, Y., Liu, S., 2020. Low Dose CT Image Reconstruction Based on Structure Tensor Total Variation Using Accelerated Fast Iterative Shrinkage Thresholding Algorithm. *Sensors*, 20(6). https://www.mdpi.com/1424-8220/20/6/1647.

Zeng, D., Zhang, X., Bian, Z., Huang, J., Zhang, H., Lu, L., Lyu, W., Zhang, J., Feng, Q., Chen, W., Ma, J., 2016. Cerebral perfusion computed tomography deconvolution via structure tensor total variation regularization. *Medical Physics*, 43.